

1 **Allosteric Activation of SENP1 by SUMO1 β -Grasp Domain Involves**
2 **a Dock-and-Coalesce Mechanism**

3

4 Jingjing Guo¹ and Huan-Xiang Zhou^{2*}

5 ¹Henan Engineering Research Center of Chiral Hydroxyl Pharmaceuticals, School of
6 Chemistry and Chemical Engineering, Henan Normal University, Xinxiang, Henan
7 453007, PR China;

8 ²Department of Physics and Institute of Molecular Biophysics, Florida State
9 University, Tallahassee, Florida 32306, USA

10 *Correspondence: hzhou4@fsu.edu

11

12

13 **Abstract** Small ubiquitin-related modifiers (SUMOs) are conjugated to proteins to
14 regulate a variety of cellular processes. SENPs are cysteine proteases with a catalytic
15 center located within a channel between two subdomains that catalyzes SUMO
16 C-terminal cleavage for processing of SUMO precursors and de-SUMOylation of
17 target proteins. The β -grasp domain of SUMOs binds to an exosite cleft, and
18 allosterically activates SENPs via an unknown mechanism. Our molecular dynamics
19 simulations showed that binding of the β -grasp domain induces significant
20 conformational and dynamic changes in SENP1, including widening of the exosite
21 cleft and quenching of nanosecond dynamics in all but a distal region. A
22 dock-and-coalesce mechanism emerges for SENP-catalyzed SUMO cleavage: the
23 wedging of the β -grasp domain enables the docking of the proximal portion of the
24 C-terminus and the strengthened cross-channel motional coupling initiates
25 inter-subdomain correlated motions to allow for the distal portion to coalesce around
26 the catalytic center.

27

28 **Introduction**

29 Whereas conjugation with ubiquitin targets proteins for degradation, conjugation with
30 small ubiquitin-related modifiers (SUMOs), or SUMOylation, is involved in various
31 cellular processes and required for normal growth and development in all eukaryotes
32 (Johnson, 2004). Although there is only 18% sequence identity between ubiquitin and
33 SUMO1 (the founding member of the SUMO family (Okura et al., 1996)), their
34 structured domains share a common fold known as β -grasp, in which five β -strands
35 wrap around an α -helix (Bayer et al., 1998) (Figure 1). SUMOylation, like
36 ubiquitination, is through an isopeptide linkage between a conserved Gly-Gly motif at
37 the C-terminus of SUMOs and a lysine sidechain on target proteins. All SUMOs are
38 translated as precursors that are first processed by the SENP family of SUMO-specific
39 proteases, whereby a short C-terminal extension is cleaved to expose the reactive
40 Gly-Gly motif. Like the much better-known posttranslational modification
41 phosphorylation, SUMOylation is reversible, and de-SUMOylation is also catalyzed
42 by SENPs (Yeh, 2009). The catalytic activity of SENPs on short peptide substrates is
43 low, likely to avoid off-target cleavage, and is substantially enhanced by the β -grasp
44 domain of SUMOs (Mikolajczyk et al., 2007). The mechanism of this allosteric
45 activation has remained poorly understood. The aim of the present study was to gain
46 insight into the allosteric mechanism through extensive molecular dynamics (MD)
47 simulations.

48 The human genome encodes three SUMOs (SUMO1, SUMO2, and SUMO3) and
49 six SUMO-specific SENPs (SENP1, SENP2, SENP3, SENP5, SENP6, and SENP7).
50 SENPs belong to the cysteine protease superfamily, and regulate both physiological
51 and pathological processes mediated by SUMOylated proteins (Yeh, 2009). As an
52 example, hypoxia (i.e., low oxygen), a condition common to fetal development and
53 tumorigenesis, induces the nuclear entry and SUMOylation of hypoxia-inducible
54 factor 1 α (HIF1 α) (Cheng et al., 2007). SUMOylated HIF1 α is subject to
55 ubiquitin-dependent degradation, and hence deSUMOylation of HIF1 α by SENP1 is
56 central to hypoxia response. For this and other reasons SENP1 is overexpressed

57 during the development of prostate cancer, and has emerged as a potential therapeutic
58 target (Cheng et al., 2006; Bawa-Khalfe et al., 2010; Wang et al., 2013). Several types
59 of SENP inhibitors have been identified, including SUMO variants or C-terminal
60 fragments tethered with electrophilic traps (Hemelaar et al., 2004; Borodovsky et al.,
61 2005; Dobrotă et al., 2012) and small molecules (Albrow et al., 2011; Ponder et al.,
62 2011; Chen et al., 2012; Madu et al., 2013). The therapeutic value of these inhibitors
63 is limited by covalent linkage with the catalytic cysteine residue, low specificity, or
64 low potency. Better understanding of the mechanism for the allosteric activation of
65 SENPs may lead to new avenues for drug development.

66 Structural studies have shown that SENP catalytic domains only undergo localized
67 conformational rearrangements upon binding SUMOs (as precursors, processed
68 products, or SUMO conjugates), and that SENP-SUMO interactions are largely
69 similar during precursor processing and deSUMOylation (Reverter and Lima, 2004;
70 Reverter and Lima, 2006; Shen et al., 2006a; Shen et al., 2006b; Xu et al., 2006;
71 Alegre and Reverter, 2014). In SENP1, the catalytic triad comprises residues His533,
72 Asp550, and Cys603 (Figure 1). The catalytic domain (residues 419-644) consists of
73 eight α -helices and seven β -strands, divided into two subdomains. The lower
74 subdomain contains the α 1, α 2, and α 8 helices and the β 1- β 2 hairpin, while the upper
75 subdomain contains the α 4- α 6 helices and the β 3- β 7 sheet. The two remaining
76 helices, α 3 and α 7, glue the two subdomains and also form the bottom of a channel
77 where the extended C-terminus of SUMO1 lies and the catalytic triad is situated.
78 Three loops, including residues 464-466 between α 2 and α 3, residues 530-533
79 between β 4 and β 5, and residues 599-602 between β 7 and α 7, line the channel and
80 likely undergo transient motions during the entrance of the SUMO C-terminus into
81 the channel. Hereafter these loops are referred to as loopA, loopB, and loopC,
82 respectively. One tryptophan residue, Trp534, floors the substrate while another,
83 Trp465, forms a lid over its conserved Gly-Gly motif. The burial of the catalytic
84 center in the channel and consequently the transient motions around the channel
85 necessary for proper alignment of the substrate with respect to the catalytic center
86 may contribute to the low catalytic activity of SENPs on short peptides.

87 The β -grasp domain of SUMO1 binds into a large cleft to the side (hereafter the
88 exosite), and makes separate contacts with the two subdomains of SENP1: the β 1- β 2
89 hairpin in the lower subdomain and the α 4- α 5 helices in the upper subdomain
90 (Figure 1). An insertion in the β 1- β 2 hairpin of SENP2 that extended the interface
91 with SUMO2 resulted in no other change in the structure of the catalytic domain but
92 nevertheless increased its catalytic activity (Alegre and Reverter, 2014). Given that
93 SENPs generally lack major conformational changes upon binding SUMOs, there is
94 no simple explanation for the allosteric activation of SENPs by the β -grasp domain of
95 SUMOs. In this context, we note that, in addition to conformational changes, the
96 possibility that changes in conformational dynamics can mediate allosteric effects has
97 received attention in the recent literature (Guo and Zhou, 2016).

98 Similar to SENPs, deubiquitinating enzymes (DUBs) in the cysteine protease class
99 also have very low catalytic activity on short peptide substrates (Dang et al., 1998).
100 Although the catalytic domains of DUBs in different families have different structural
101 scaffolds, they all contain a catalytic channel that bears resemblance to that in SENPs
102 (Hu et al., 2002; Misaghi et al., 2005; Messick et al., 2008). The resemblance further
103 extends to the positioning of the ubiquitin domain in the exosite. It may thus be
104 expected that allosteric activation mechanisms of SENPs and DUBs share certain
105 similarities.

106 A major step toward elucidating the allosteric activation of SENP1 by the β -grasp
107 domain of SUMO1 was taken in a recent study (Chen et al., 2014). These authors
108 confirmed the ability of a pre-bound β -grasp domain, as contained in a truncated
109 SUMO1 construct (residues 1-92, hereafter referred to as trunSUMO1), to enhance
110 the SENP1 catalytic activity on a short peptide substrate, and further traced the
111 enhancement solely to an increase in k_{cat} . Their NMR data showed that trunSUMO1
112 binding yielded a gradient in backbone amide chemical shift perturbations (CSPs)
113 emanating from the exosite cleft to the catalytic center. Significant sidechain methyl
114 CSPs were also observed on six residues that dotted the region from the exosite cleft
115 to the catalytic center, which indicated to the authors that the allosteric effect was
116 propagated through the hydrophobic core. Their Carr-Purcell-Meiboom-Gill (CPMG)

117 relaxation dispersion data showed that trunSUMO1 binding enhanced
118 microsecond-millisecond (μ s-ms) dynamics for residues around the catalytic center,
119 suggesting a realignment of these residues. Chen et al.'s NMR data provided
120 residue-level information, but their sparseness precluded a full picture on how the
121 allosteric communication occurred in SENP1 upon binding trunSUMO1.

122 Here we present an atomistic picture for the allosteric communication derived
123 from MD simulations. The simulations showed that trunSUMO1 binding induces
124 significant conformational and dynamic changes in SENP1, including widening of the
125 exosite cleft and quenching of nanosecond (ns) dynamics in all but a distal region.
126 Calculated backbone amide and sidechain methyl CSPs are in broad agreement with
127 the experimental data of Chen et al. (2014) but more pronounced, and our sidechain
128 CSPs clearly identify two hydrophobic pathways, each within a subdomain, for
129 allosteric communication from the exosite cleft to the catalytic center. The β -grasp
130 domain, by serving as a bridge that links the two exosite interface regions, strengthens
131 intra- and inter-subdomain motional coupling, which in turn may be the underlying
132 reason for the quenching of ns dynamics and potentially may also be the instigator of
133 inter-subdomain μ s-ms dynamics (Guo and Zhou, 2015). The concerted action of the
134 β -grasp induced conformational and dynamic changes is captured by a
135 dock-and-coalesce mechanism for SENP-catalyzed SUMO cleavage, whereby the
136 wedging of the β -grasp domain into the exosite cleft enables the docking of the
137 proximal portion of the C-terminus, and the strengthened cross-channel coupling
138 initiates inter-subdomain correlated motions to allow for the distal portion to coalesce
139 around the catalytic center.

140

141 **Results**

142 We carried out three replicate explicit-solvent MD simulations for apo SENP1, for
143 SENP1 bound with trunSUMO1, and for SENP1 bound with the full-length SUMO1
144 precursor (referred to as preSUMO1 hereafter). For each system, the three simulations
145 accumulated 1.7 μ s of total time and are denoted as sim1, sim2, and sim3.

146

147 **β -Grasp binding induces wider exosite cleft and stronger inter-subdomain**
148 **contact**

149 To compare the conformational sampling by the apo, trunSUMO1-bound, and
150 preSUMO1-bound forms of SENP1, we carried out principal component analysis on
151 the replicate simulations of the three systems. The distributions of conformations in
152 the plane of the first two principal components (PC1 and PC2), translated to free
153 energy surfaces according to the Boltzmann relation, are displayed in Figure 2 –
154 figure supplement 1a. The three systems cover overlapping as well as distinct regions
155 in conformational space. The apo form samples disconnected free energy basins, in
156 contrast to the two bound forms, indicating a decrease in flexibility upon β -grasp
157 binding (see below).

158 Both PC1 and PC2 feature prominent displacements in the two exosite interface
159 regions and in the loops lining the catalytic channel (Figure 2 – figure supplement
160 1b,c). Relative to the apo form, the two bound forms move along positive PC1 and
161 PC2, both of which involve the moving apart between the two interface regions and
162 the opposite movements of loopA and loopB with respect to the β -grasp domain. We
163 hence directly monitored the relative motions between the two interface regions and
164 between the three channel-lining loops (Figure 2). The distributions of the cleft
165 distance, defined as between the centers of heavy atoms of the interface residues
166 448-453 and 506-513 (shown as mauve in Figure 2a), are displayed in Figure 2b for
167 the three forms of SENP1. The mean and standard deviation of the cleft distance
168 change from 22.4 ± 1.5 Å for the apo form to 23.1 ± 0.5 Å and 22.6 ± 1.5 Å for the
169 trunSUMO1-bound and preSUMO1-bound forms, respectively, indicating widening
170 of the exosite cleft upon β -grasp binding (Figure 2 – figure supplement 2a,b).

171 To characterize the movements of the three channel-lining loops, we defined a
172 coordinate system attached to the $\alpha 3$ and $\alpha 7$ helices, which form the bottom of the
173 channel (Figure 2a). In the coordinate system, the z axis is along the helical axis of $\alpha 7$
174 (as defined by the vector from the C α center of residues 612–615 to the C α center of
175 residues 604–607); the x axis goes through the C α center of $\alpha 3$ residues 469-480 and

176 hence points to the exosite cleft; and the y axis points into the upper subdomain. None
177 of the three loops exhibits any overt movement along z , so we focus on the differences
178 among the three forms of SENP1 in the distributions of the $C\alpha$ center x and y
179 coordinates of the three loops (Figure 2c and Figure 2 – figure supplement 2a,b).
180 Relative to the apo form, the two bound form show similar movements for both loopA
181 and loopB, the former away from the exosite cleft (i.e., decreasing x) and toward the
182 upper subdomain (i.e., increasing y) while the latter toward the cleft and away from
183 the channel (i.e., increasing x and y); loopC moves in opposite directions in the two
184 bound forms but perhaps that is accidental due to the long distance from the binding
185 interface. The movement of loopA (toward $\alpha 7$) leads to stronger inter-subdomain
186 contact; the x component of loopB's movement has a similar effect, while the y
187 component may create space for the docking of the proximal portion of a C-terminus
188 when tethered to the β -grasp domain.

189 The stronger inter-subdomain contact induced by β -grasp binding can be further
190 illustrated by the movement of the sidechain of the channel lid residue, W465 (Figure
191 2d). In apo SENP1 this sidechain samples a broad range of positions, but in
192 preSUMO1-bound SENP1 it stays stably near the top of $\alpha 7$ (on the sub- μ s timescale);
193 the situation is intermediate in trunSUMO1-bound SENP1.

194

195 **Nanosecond dynamics of SENP1 is quenched upon β -grasp binding**

196 As noted above, the narrowing of accessible conformational regions upon β -grasp
197 binding suggests a decrease in flexibility, i.e., quenching of ns dynamics. To compare
198 the residue-specific flexibilities among the three forms of SENP1, we calculated their
199 $C\alpha$ root-mean-square fluctuations (RMSFs). Relative to apo SENP1, the two bound
200 forms both show decreased flexibility throughout most of the amino acid sequence,
201 except for the N- and C-terminal segments (Figure 3a).

202 To visualize how the changes in RMSF are distributed spatially, we display them
203 according to a color scale on the structures of the two bound forms (Figure 3b,c). In
204 both systems, rigidification propagates from the exosite cleft to the entire upper
205 subdomain and to most of the lower subdomain. The rigidification is compensated to

206 some extent by higher flexibility in the distal region of the lower subdomain,
207 comprising the N- and C-terminal segments. Therefore the allosteric effects elicited
208 by the β -grasp domain include both the stronger inter-subdomain contact and the
209 quenching of ns dynamics in all but a distal region.

210

211 **Calculated sidechain methyl CSPs identify two hydrophobic pathways for** 212 **allosteric communication**

213 Chen et al. (2014) measured the backbone amide CSPs of SENP1 upon trunSUMO1
214 binding. Their CSPs can be described as a gradient emanating from the exosite cleft to
215 the catalytic center (Figure 4a), a pattern that is somewhat similar to that of the
216 changes in RMSF (Figure 3b). In addition, they observed significant sidechain methyl
217 CSPs on six residues, including Leu450, Val501, Val 509, V516, Val518, and ValV532,
218 which sparsely occupy the region from the exosite cleft to the catalytic center (Figure
219 4a).

220 To compare with these NMR results, we calculated the chemical shifts of
221 backbone amides and sidechain methyls on the apo and trunSUMO1-bound SENP1
222 simulations. The resulting CSPs are displayed in Figure 4b. Overall they agree well
223 with the experimental data, but are more pronounced. The calculated backbone amide
224 CSPs spread all the way to the back, in both subdomains. The calculation identifies
225 three of the six experimentally detected residues as well as 12 others as having
226 significant sidechain methyl CSPs (> 0.08 ppm). Interestingly, with the 12 additional
227 residues, two hydrophobic pathways emerge, each connecting an exosite interface
228 region in one subdomain to the catalytic center. Chemical shifts are a measure of both
229 conformational and dynamics effects. Hence the sidechain methyl CSPs are a
230 manifestation of the conformational and dynamic changes induced by β -grasp binding,
231 and the hydrophobic pathways may represent short paths over which allosteric effects
232 are propagated from the exosite cleft to the catalytic center.

233

234 **Strengthened intra- and inter-subdomain motional coupling underlies quenching** 235 **of ns dynamics**

Community analysis is a way to reveal the pattern of motional coupling within a protein, based on residue-residue physical contact and positional correlation during an MD simulation (Sethi et al., 2009). A protein structure is partitioned into communities, within which residues form dense contacts but between which residues form sparse contacts. The strength of coupling, or betweenness, between two communities is determined by the magnitudes of positional correlations within networks of contacting residues.

Results of our community analysis are displayed in Figure 5 for apo and trunSUMO1-bound sim1, and in Figure 5 – figure supplements 1 and 2 for the other two replicate simulations. Very similar community structures are obtained from the replicate simulations of each system, so here we focus on sim1. In all cases, five major communities (numbered 1 to 5) can be recognized for SENP1, anchored by **$\beta 1\beta 2$** and **$\alpha 2$** ; **$\alpha 3$** ; **$\alpha 4\alpha 5$** ; **$\alpha 6$** and various parts of $\beta 4$ - $\beta 7$; and **$\alpha 7$** , respectively, and possibly containing other segments. In the apo form, in addition to these five major communities, four minor communities (numbered 1', 2', 4', and 4'') are also formed. In the trunSUMO1-SENP1 complex, SENP1 is partitioned only to the five major communities, with the minor communities absorbed. In particular, communities 4, 4', and 4'' in apo SENP1 coalesce into a single community upon trunSUMO1 binding.

Moreover, the inter-community betweennesses are also strengthened, especially between the two communities, 2 and 5, anchored by the two central helices (**$\alpha 3$** and **$\alpha 7$** , respectively) and community 1 in the lower subdomain and community 4 in the upper subdomain. This strengthened inter-community coupling is in line with the stronger inter-subdomain contact noted above. It comes about because the β -grasp domain couples strongly to both subdomains. Therefore, the β -grasp domain, by serving as a bridge linking the two exosite interface regions, strengthens the motional coupling both within and between the subdomains of SENP1. A similar bridging role was identified for a peptide in inducing inter-domain allosteric communication in Pin1 (Guo et al., 2015).

With the strengthened intra-subdomain coupling upon trunSUMO1 binding, it can be expected that allosteric communication from the exosite cleft to the catalytic center

266 becomes more effective. The effectiveness of allosteric communication between two
267 sites can be measured by the lengths, defined using the residue-residue positional
268 correlations (i.e., stronger correlations correspond to shorter lengths), of paths
269 connecting the sites. Indeed, the path lengths from the two exosite interface regions to
270 the catalytic center are shorter in the trunSUMO1-bound form than in the apo form.
271 This result is in line with the two hydrophobic pathways identified by sidechain
272 methyl CSPs.

273 The simultaneous occurrence of strengthened intra- and inter-subdomain coupling
274 and quenching of ns dynamics observed here on SENP1 upon binding an allosteric
275 activator conforms to a pattern previously recognized from a number of other proteins
276 (including Pin1) in which conformational dynamics plays a prominent role in
277 mediating allosteric communication (Guo and Zhou, 2015). This pattern was
278 explained by a dynamic model of allostery. According to this model, fast motions (e.g.,
279 those on a ns timescale) are uncorrelated; an allosteric activator strengthens
280 inter-community coupling, which in turn leads to quenching of fast motions. The
281 strengthened coupling here comes about because the β -grasp domain serves as a
282 bridge that links the two interfacial regions. The model further predicts another
283 dynamic effect, i.e., slower (e.g., μ s-ms), cross-community correlated motions are
284 initiated. Indeed, Chen et al.'s CPMG data for residues around the catalytic center
285 indicated enhanced μ s-ms conformational exchange upon trunSUMO1 binding (Chen
286 et al., 2014).

287

288 **Allosteric effects can be reproduced by restraining the two exosite interface** 289 **regions at an widened separation**

290 The results presented above lead to the hypothesis that the conformational and
291 dynamic effects of β -grasp binding are achieved through increasing the exosite cleft
292 distance and then rigidly holding the two interface regions at the widened separation.
293 As demonstrated previously for Pin1 (Guo et al., 2015), this type of hypotheses can be
294 tested by restrained MD simulations. Specifically, we ran an apo simulation but
295 restrained the two exosite interface regions (i.e., the β 1 β 2 hairpin in the lower

subdomain and the $\alpha 4\alpha 5$ helices in the upper subdomain) to their conformation from a snapshot in trunSUMO1-bound sim1, in which the exosite cleft distance is at a widened 23.9 Å (Figure 6a).

The simulation of this control system reproduces the main conformational and dynamic effects of β -grasp binding. The three channel-lining loops in the control system move in essentially the same ways as those in the trunSUMO1-bound form (compare Figure 6 – figure supplement 1a,b with Figure 2c and Figure 2 – figure supplement 2b). The RMSF of the control system (Figure 6b) also shows a similar albeit slightly more pronounced decrease, indicating quenching of ns dynamics, for most of the SENP1 structure, including all the three channel-lining loops. Lastly the calculated backbone amide CSPs of the control system have a similar gradient to that of the trunSUMO1-bound form, and the calculated sidechain methyl CSPs again identify two hydrophobic pathways that may propagate allosteric effects from the exosite cleft to the catalytic center (Figure 6c).

Discussion

Through extensive MD simulations, we have found that SUMO1 β -grasp binding to SENP1 induces significant conformational and dynamic effects, including the widening of the exosite cleft and the quenching of ns dynamics in all but a distal region. The calculated CSPs are in broad agreement with the NMR data of Chen et al. (2014) but our results overall present a deeper, atomistic picture for the allosteric communication from the exosite cleft to the catalytic center. We conclude that the wedging into the exosite cleft and the bridging between the two exosite interface regions by the β -grasp domain are the underlying reason for the widened exosite cleft and the quenched fast dynamics, and may also be the instigator of inter-subdomain slow motions. Enhanced μ s-ms conformational exchange has indeed been observed in CPMG experiments on trunSUMO1-bound SENP1 (Chen et al., 2014). Our findings have broad implications for the mechanism of allosteric activation of SENPs by SUMOs, the SUMO paralogue specificity of SENPs, and the development of drugs

325 targeting SENPs.

326

327 **A dock-and-coalescence mechanism for SENP-catalyzed SUMO cleavage**

328 The concerted action of the β -grasp induced conformational and dynamic changes is
329 expected to help both the binding step and the subsequent catalytic step for
330 trunSUMO1-bound SENP1 reacting with an isolated peptide substrate. First,
331 widening of the exosite cleft may enhance the rate at which the substrate binds to the
332 catalytic center, although this effect may not be detectable in an enzymatic assay if the
333 binding does not rate-limit the overall enzymatic reaction. Second, initiation of slow
334 conformational dynamics may facilitate the proper alignment of the substrate around
335 the catalytic residues. These putative effects can explain the observation of Chen et al.
336 (2014) that trunSUMO1 enhances the SENP1 catalytic activity on a peptide substrate
337 through increasing k_{cat} .

338 In SENP-catalyzed SUMO cleavage for processing of SUMO precursors and
339 de-SUMOylation of target proteins, the C-terminal substrate is tethered to the β -grasp
340 domain via an extended linker. Tethering can also help both the binding step and the
341 subsequent catalytic step. The binding of a substrate-containing SUMO (i.e., a
342 precursor or SUMO conjugate) likely occurs in a sequential manner: the β -grasp
343 domain first wedges into the exosite cleft and the C-terminus then docks into the
344 catalytic channel. Tethering can facilitate this binding by correctly orienting the
345 C-terminal substrate. This effect and the β -grasp induced widening of the exosite cleft
346 together may speed up the docking of the C-terminus into the catalytic channel
347 sufficiently as to make the full binding step rate-limited by the initial wedging of the
348 β -grasp into the exosite. Tethering can also reinforce the motional coupling between
349 the exosite interface regions and the channel-lining loops. This may in turn intensify
350 the slow conformational dynamics that facilitates the proper alignment of the
351 substrate around the catalytic residues, thereby accelerating the catalytic step.

352 In previous studies we have put forward a docking-and-coalesce mechanism to
353 describe the binding of intrinsically disordered proteins, which, similar to the
354 disordered SUMO C-terminus, usually form extended conformations on their targets

355 (Qin et al., 2011; Zhou et al., 2012). Here we adapt this mechanism to describe the
356 steps of SENP-catalyzed SUMO cleavage reaction just before the actual cut of the
357 (iso)peptide bond (Figure 7). The process starts with the wedging of the SUMO
358 β -grasp domain into the SENP exosite cleft. This wedging widens the separation
359 between and also tightly links the two exosite interface regions. The widening of the
360 exosite cleft enables the docking of the proximal portion of the C-terminus into the
361 catalytic channel. Moreover, the wedged β -grasp domain strengthens the motional
362 coupling within and between the two subdomains of SENP, and the newly docked
363 proximal portion of the SUMO C-terminus reinforces this coupling. According to a
364 theoretical model (Guo and Zhou, 2015), the strengthened coupling sets up the
365 condition for the emergence of inter-subdomain correlated motions, which finally
366 allow for the distal portion of the SUMO C-terminus to align properly around the
367 catalytic center for bond cleavage.

368 The preceding dock-and-coalesce mechanism differs from the previous generic
369 version (Qin et al., 2011; Zhou et al., 2012) by the cooperation between a structure
370 domain (i.e., the β -grasp domain) and a disordered region (i.e., the C-terminus) of the
371 substrate protein and by the prominent role of allosteric communication within the
372 target protein. In addition, the end result here is the transition-state complex for a
373 catalytic reaction as opposed to a ground-state complex. Certain aspects of the
374 mechanism presented here have been suggested previously by Shen et al. (2006a),
375 including the stimulation of catalytic channel opening by SUMO binding and the
376 facilitation of substrate alignment by cross-channel dynamics, without elaboration.
377 Lastly the dock-and-coalesce mechanism may not only provide a qualitative
378 description of the individual steps but also serve as a framework for quantitative
379 calculations of kinetic rate constants (see next).

380

381 **Contributions of exosite SENP-SUMO interactions to paralogue specificity**

382 The catalytic activities of a particular SENP can vary toward different SUMO
383 paralogues (Reverter and Lima, 2006; Shen et al., 2006a; Hickey et al., 2012). For
384 example, SENP1 processes preSUMO1 and deconjugates SUMO1 and SUMO2

385 conjugates with similar rates, but processes the SUMO2 precursor with a 25-fold
386 lower k_{cat} (Shen et al., 2006a). The decrease in k_{cat} was attributed to a compromised fit
387 between the C-terminal extension and the catalytic channel. On the other hand, in
388 either processing or deconjugation, SENP2 discriminates between SUMO1 and
389 SUMO2 not by k_{cat} but by K_M (Reverter and Lima, 2006). An approximately 10-fold
390 lower K_M for SUMO2 was attributed to an extended exosite interface.

391 The dock-and-coalesce mechanism presented above now allows us to more
392 clearly delineate the contributions of exosite interactions to paralogue specificity. Two
393 consequences can be expected of the more extensive exosite interactions of SENP2
394 with SUMO2 than with SUMO1. First, stronger electrostatic attraction across the
395 exosite interface quickens the initial wedging of the SUMO2 β -grasp domain into the
396 exosite and slows down the reverse process. Second, the more extensive exosite
397 interactions likely cause stronger allosteric effects of the wedged β -grasp domain,
398 resulting in faster docking of the SUMO2 C-terminus into the catalytic channel. These
399 two consequences together may explain the lower K_M for SUMO2 than for SUMO1.
400 A precedent of the second consequence occurred in Pin1, where peptides bound at an
401 inter-domain exosite were identified to serve a bridging role similar to the one
402 proposed here for the β -grasp domain; a peptide with more extensive across-domain
403 interactions indeed induced stronger allosteric effects (Guo et al., 2015; Guo and
404 Zhou, 2015).

405 Here the expectation for stronger allosteric effects is specifically supported by the
406 observation that a pre-bound SUMO2, but not SUMO1, β -grasp domain enhanced the
407 SENP2 catalytic activity on a peptide substrate (Mikolajczyk et al., 2007). A similar
408 causal link between strengthened exosite interactions and strengthened allosteric
409 effects may be at play for a SENP2 mutant that was designed by grafting an insertion
410 in the $\beta 1$ - $\beta 2$ hairpin from SENP6 (Alegre and Reverter, 2014). The insertion extended
411 the exosite lower interface and increased the proteolytic activity of SENP2 for some
412 SUMO2 conjugates.

413

414 **SENP exosite as target site for drug development**

415 Inhibitors that target the catalytic center of SENPs have limited therapeutic value due
416 to covalent linkage with the catalytic cysteine residue, low specificity, or low potency.
417 The foregoing discussion suggests that the exosite may be another potential target site
418 for drug development. Suppression and elevation of SENP activities may both be
419 desired (under different pathological conditions) and can be achieved by disrupting
420 and strengthening exosite SENP-SUMO interactions, respectively. Small molecules
421 that bind at sites deeply into the SENP-SUMO interface can have a disruptive effect
422 (Kumar and Zhang, 2013), whereas those bind over both SENP and SUMO can lock
423 and strengthen their interactions.

424

425 **Methods**

426 **Molecular dynamics simulation protocols**

427 MD simulations were carried out for three systems: apo SENP1, SENP1-trunSUMO1
428 complex, and SENP1-preSUMO1 complex. The starting structures of the first and
429 third systems were from PDB entries 2CKG (Shen et al., 2006b) and 2IY1 (Shen et al.,
430 2006a), respectively; the latter upon removing the C-terminal 9 residues starting from
431 Glu93 was used as the starting structure of the SENP1-trunSUMO1 complex.

432 Three replicate simulations were performed for each system. sim1 and sim2 were
433 performed in NAMD 2.9 (Phillips et al., 2005) using the CHARMM 36 force field
434 (Brooks et al., 2009; Vanommeslaeghe et al., 2010), while sim3 was carried out in
435 AMBER with the AMBER99SB force field ([Hornak et al., 2006](#)). Each system was
436 placed in a water box with a 10-Å buffer zone. Appropriate numbers of Na⁺ and Cl⁻
437 were added to neutralize proteins and produce a NaCl concentration of 50 mM. For
438 the NAMD simulations, the van der Waals cut-off distance was 12 Å with a switching
439 distance of 10 Å; for AMBER simulations, the cutoff distance for non-bonded
440 interactions was 10 Å. The particle mesh Ewald was used for computing the Coulomb
441 interactions under the periodic boundary condition.

442 Before starting a simulation, the solvated system was energy minimized at three
443 stages, first with either the whole protein molecule(s) or backbone atoms restrained

444 and then without any restraint. After a 50-ps equilibration, the simulation was
445 continued at constant pressure (1 bar) and constant temperature (300 K), at a 2-fs
446 timestep.

447 The simulation times of sim1, sim2, and sim3 were 300, 400, and 1000 ns,
448 respectively, for each system. sim2 and sim3 were performed using GPU acceleration.
449 The last 150 ns (saved at 2-ps intervals) of sim1 and sim2 and last 300 ns (saved at
450 5-ps intervals) of sim3 were used for analyses.

451 One more simulation, of a control system, was also carried out. This started from
452 the snapshot at 200 ns of apo sim1, but with the heavy atoms of the interface regions,
453 $\beta 1\beta 2$ (residues 443-453) and $\alpha 4\alpha 5$ (residues 496-514), restrained to their
454 conformation in the snapshot at 200 ns of trunSUMO1-bound sim1. The force
455 constant was 2 kcal/Å² for each restrained atom.

456

457 **Calculation of Chemical Shift Perturbations**

458 The SHIFTX2 program (Han et al., 2011) was used to calculate diamagnetic ¹H, ¹³C
459 and ¹⁵N chemical shifts on SENP1 coordinates sampled from the replicate simulations
460 for each system (see next). The CSPs of backbone amides and sidechain methyls were
461 calculated as $\sqrt{(0.154 \cdot \Delta\delta_N)^2 + (\Delta\delta_H)^2}$ and $\sqrt{(0.341 \cdot \Delta\delta_C)^2 + (\Delta\delta_H)^2}$,
462 respectively (Chen et al., 2014), where $\Delta\delta_X$, denotes the chemical shift differences
463 between apo and SUMO1-bound SENP1 for nucleus X.

464

465 **Combination of Replicate Simulations**

466 The three replicate simulations for each system were combined to ensure
467 reproducibility of reported results. The principal component analysis was done after
468 pooling the conformations (every other saved ones) from all the three simulations,
469 using C α coordinates of SENP1 residues 429-637. For distributions of the cleft
470 distance and loop movements, histograms were calculated using all the snapshots
471 saved in the three replicate simulations. Chemical shifts were predicted separately for
472 each simulation (using every 15th saved conformation in sim1 or sim2 or every 10th

473 conformation in sim3), and the results from the three simulations were then averaged.
474 For RMSF, analysis was done over non-overlapping 50-ns windows (of which there
475 were 3, 3, and 6, respectively, in sim1, sim2, and sim3). Results were first averaged
476 over these windows in each simulation, and then averaged again over the three
477 replicate simulations. Finally community analysis was done separately for each
478 replicate simulation.

479

480 **Competing interests**

481 The authors declare that no competing interests exist.

482

483 **Acknowledgments**

484 We thank Dr. Yuan Chen for introducing the SENP1 allostery problem to us. This
485 work was supported by National Institutes of Health Grants GM058187 and
486 GM118091.

487

488 **References**

- 489 Albrow, VE, Ponder, EL, Fasci, D, Békés, M, Deu, E, Salvesen, GS, and Bogyo, M.
490 2011. Development of small molecule inhibitors and probes of human SUMO
491 deconjugating proteases. *Chemistry & biology* **18**: 722-732.
- 492 Alegre, KO, and Reverter, D. 2014. Structural insights into the SENP6 Loop1
493 structure in complex with SUMO2. *Protein Sci* **23**: 433-441.
- 494 Bawa-Khalfe, T, Cheng, J, Lin, S-H, Ittmann, MM, and Yeh, ET. 2010. SENP1
495 induces prostatic intraepithelial neoplasia through multiple mechanisms. *Journal of*
496 *Biological Chemistry* **285**: 25859-25866.
- 497 Bayer, P, Arndt, A, Metzger, S, Mahajan, R, Melchior, F, Jaenicke, R, and Becker, J.
498 1998. Structure determination of the small ubiquitin-related modifier SUMO-1.
499 *Journal of molecular biology* **280**: 275-286.
- 500 Borodovsky, A, Ovaa, H, Meester, WJ, Venanzi, ES, Bogyo, MS, Hekking, BG,

501 Ploegh, HL, Kessler, BM, and Overkleeft, HS. 2005. Small - Molecule Inhibitors and
 502 Probes for Ubiquitin - and Ubiquitin - Like - Specific Proteases. *Chembiochem* **6**:
 503 287-291.

504 Brooks, BR, Brooks, CL, MacKerell, AD, Nilsson, L, Petrella, RJ, Roux, B, Won, Y,
 505 Archontis, G, Bartels, C, and Boresch, S. 2009. CHARMM: the biomolecular
 506 simulation program. *Journal of computational chemistry* **30**: 1545-1614.

507 Chen, CH, Namanja, AT, and Chen, Y. 2014. Conformational flexibility and changes
 508 underlying activation of the SUMO-specific protease SENP1 by remote substrate
 509 binding. *Nat Commun* **5**: 4968.

510 Chen, Y, Wen, D, Huang, Z, Huang, M, Luo, Y, Liu, B, Lu, H, Wu, Y, Peng, Y, and
 511 Zhang, J. 2012. 2-(4-Chlorophenyl)-2-oxoethyl 4-benzamidobenzoate derivatives, a
 512 novel class of SENP1 inhibitors: Virtual screening, synthesis and biological
 513 evaluation. *Bioorg Med Chem Lett* **22**: 6867-6870.

514 Cheng, J, Bawa, T, Lee, P, Gong, L, and Yeh, ET. 2006. Role of desumoylation in the
 515 development of prostate cancer. *Neoplasia* **8**: 667-676.

516 Cheng, J, Kang, X, Zhang, S, and Yeh, ET. 2007. SUMO-specific protease 1 is
 517 essential for stabilization of HIF1alpha during hypoxia. *Cell* **131**: 584-595.

518 Dang, LC, Melandri, FD, and Stein, RL. 1998. Kinetic and Mechanistic Studies on the
 519 Hydrolysis of Ubiquitin C-Terminal 7-Amido-4-Methylcoumarin by Deubiquitinating
 520 Enzymes. *Biochemistry* **37**: 1868-1879.

521 Dobrotă, C, Fasci, D, Hădăde, ND, Roiban, GD, Pop, C, Meier, VM, Dumitru, I,
 522 Matache, M, Salvesen, GS, and Funeriu, DP. 2012. Glycine Fluoromethylketones as
 523 SENP - Specific Activity Based Probes. *ChemBioChem* **13**: 80-84.

524 Guo, J, Pang, X, and Zhou, HX. 2015. Two pathways mediate interdomain allosteric
 525 regulation in pin1. *Structure* **23**: 237-247.

526 Guo, J, and Zhou, H-X. 2016. Protein Allostery and Conformational Dynamics.
 527 *Chemical Reviews*.

528 Guo, J, and Zhou, HX. 2015. Dynamically Driven Protein Allostery Exhibits
 529 Disparate Responses for Fast and Slow Motions. *Biophys J* **108**: 2771-2774.

530 Han, B, Liu, Y, Ginzinger, SW, and Wishart, DS. 2011. SHIFTX2: significantly

531 improved protein chemical shift prediction. *Journal of Biomolecular NMR* **50**: 43-57.
 532 Hemelaar, J, Borodovsky, A, Kessler, BM, Reverter, D, Cook, J, Kolli, N, Gan-Erdene,
 533 T, Wilkinson, KD, Gill, G, and Lima, CD. 2004. Specific and covalent targeting of
 534 conjugating and deconjugating enzymes of ubiquitin-like proteins. *Molecular and*
 535 *cellular biology* **24**: 84-95.
 536 Hickey, CM, Wilson, NR, and Hochstrasser, M. 2012. Function and regulation of
 537 SUMO proteases. *Nat Rev Mol Cell Biol* **13**: 755-766.
 538 Hu, M, Li, P, Li, M, Li, W, Yao, T, Wu, JW, Gu, W, Cohen, RE, and Shi, Y. 2002.
 539 Crystal structure of a UBP-family deubiquitinating enzyme in isolation and in
 540 complex with ubiquitin aldehyde. *Cell* **111**: 1041-1054.
 541 Johnson, ES. 2004. Protein modification by SUMO. *Annu Rev Biochem* **73**: 355-382.
 542 Kumar, A, and Zhang, KYJ. 2013. Computational Investigation of SENP:SUMO
 543 Protein-Protein Interaction for Structure Based Drug Design. *Molecular Informatics*
 544 **32**: 267-280.
 545 Madu, IG, Namanja, AT, Su, Y, Wong, S, Li, YJ, and Chen, Y. 2013. Identification and
 546 characterization of a new chemotype of noncovalent SENP inhibitors. *ACS Chem Biol*
 547 **8**: 1435-1441.
 548 Messick, TE, Russell, NS, Iwata, AJ, Sarachan, KL, Shiekhata, R, Shanks, JR,
 549 Reyes-Turcu, FE, Wilkinson, KD, and Marmorstein, R. 2008. Structural basis for
 550 ubiquitin recognition by the Otul ovarian tumor domain protein. *J Biol Chem* **283**:
 551 11038-11049.
 552 Mikolajczyk, J, Drag, M, Bekes, M, Cao, JT, Ronai, Z, and Salvesen, GS. 2007. Small
 553 ubiquitin-related modifier (SUMO)-specific proteases: profiling the specificities and
 554 activities of human SENPs. *J Biol Chem* **282**: 26217-26224.
 555 Misaghi, S, Galardy, PJ, Meester, WJ, Ovaa, H, Ploegh, HL, and Gaudet, R. 2005.
 556 Structure of the ubiquitin hydrolase UCH-L3 complexed with a suicide substrate. *J*
 557 *Biol Chem* **280**: 1512-1520.
 558 Okura, T, Gong, L, Kamitani, T, Wada, T, Okura, I, Wei, CF, Chang, HM, and Yeh, ET.
 559 1996. Protection against Fas/APO-1- and tumor necrosis factor-mediated cell death by
 560 a novel protein, sentrin. *J Immunol* **157**: 4277-4281.

561 Phillips, JC, Braun, R, Wang, W, Gumbart, J, Tajkhorshid, E, Villa, E, Chipot, C,
 562 Skeel, RD, Kale, L, and Schulten, K. 2005. Scalable molecular dynamics with NAMD.
 563 *Journal of computational chemistry* **26**: 1781-1802.

564 Ponder, EL, Albrow, VE, Leader, BA, Békés, M, Mikolajczyk, J, Fonović, UP, Shen,
 565 A, Drag, M, Xiao, J, and Deu, E. 2011. Functional characterization of a SUMO
 566 deconjugating protease of Plasmodium falciparum using newly identified small
 567 molecule inhibitors. *Chemistry & biology* **18**: 711-721.

568 Qin, S, Pang, X, and Zhou, H-X. 2011. Automated Prediction of Protein Association
 569 Rate Constants. *Structure* **19**: 1744-1751.

570 Reverter, D, and Lima, CD. 2004. A Basis for SUMO Protease Specificity Provided
 571 by Analysis of Human Senp2 and a Senp2-SUMO Complex. *Structure* **12**: 1519-1531.

572 Reverter, D, and Lima, CD. 2006. Structural basis for SENP2 protease interactions
 573 with SUMO precursors and conjugated substrates. *Nat Struct Mol Biol* **13**: 1060-1068.

574 Sethi, A, Eargle, J, Black, AA, and Luthey-Schulten, Z. 2009. Dynamical networks in
 575 tRNA:protein complexes. *Proc Natl Acad Sci U S A* **106**: 6620-6625.

576 Shen, L, Tatham, MH, Dong, C, Zagorska, A, Naismith, JH, and Hay, RT. 2006a.
 577 SUMO protease SENP1 induces isomerization of the scissile peptide bond. *Nat Struct*
 578 *Mol Biol* **13**: 1069-1077.

579 Shen, LN, Dong, C, Liu, H, Naismith, JH, and Hay, RT. 2006b. The structure of
 580 SENP1-SUMO-2 complex suggests a structural basis for discrimination between
 581 SUMO paralogues during processing. *Biochem J* **397**: 279-288.

582 Vanommeslaeghe, K, Hatcher, E, Acharya, C, Kundu, S, Zhong, S, Shim, J, Darian, E,
 583 Guvench, O, Lopes, P, and Vorobyov, I. 2010. CHARMM general force field: A force
 584 field for drug - like molecules compatible with the CHARMM all - atom additive
 585 biological force fields. *Journal of computational chemistry* **31**: 671-690.

586 Wang, Q, Xia, N, Li, T, Xu, Y, Zou, Y, Zuo, Y, Fan, Q, Bawa-Khalfe, T, Yeh, E, and
 587 Cheng, J. 2013. SUMO-specific protease 1 promotes prostate cancer progression and
 588 metastasis. *Oncogene* **32**: 2493-2498.

589 Xu, Z, Chau, SF, Lam, KH, Chan, HY, Ng, TB, and Au, SW. 2006. Crystal structure
 590 of the SENP1 mutant C603S-SUMO complex reveals the hydrolytic mechanism of

591 SUMO-specific protease. *Biochem J* **398**: 345-352.
592 Yeh, ET. 2009. SUMOylation and De-SUMOylation: wrestling with life's processes. *J*
593 *Biol Chem* **284**: 8223-8227.
594 Zhou, HX, Pang, X, and Lu, C. 2012. Rate constants and mechanisms of intrinsically
595 disordered proteins binding to structured targets. *Phys Chem Chem Phys* **14**:
596 10466-10476.
597
598
599

600

601 **Figure 1.** Structure of the SENP1-SUMO1 complex (PDB entry 2IY1). SENP1 is
602 shown as gray surface and cartoon representations in the left and right panels,
603 respectively, and the closed catalytic channel is boxed and enlarged in the middle
604 panel. Sidechains of the catalytic triad and of two tryptophans shaping the catalytic
605 channels are shown as sticks. Three channel-lining loops (residues 464-466, 530-533,
606 and 599-602) are shown in orange; two exosite interface regions (residues 443-453
607 and 496-514) are shown in mauve. SUMO1 is shown in green but with the conserved
608 C-terminal Gly-Gly motif in red.

609

610 **Figure 2.** The displacements of the exosite interface regions and channel-lining loops
611 upon SUMO1 binding. (a) The regions (displayed in mauve) used for defining cleft
612 distance (indicated by double-headed arrow) and the coordinate system used for
613 defining movements of the three channel-lining loops (displayed in orange) and the
614 W465 sidechain (displayed with carbon atoms in cyan). (b) The distributions of the
615 cleft distance in the simulations of the apo and trunSUMO1- and preSUMO1-bound
616 forms of SENP1. The average value of each system is shown as dash with matching
617 color. (c) Distributions of the Ca centers of the three loops in the x - y plane. The
618 average positions of the loops in each system are shown as dots. (d) Corresponding
619 results for the center of W465 sidechain heavy atoms.

620

621 **Figure 3.** Comparison of flexibility among three systems, as measured by Ca atom
622 root-mean-square fluctuations (RMSFs). (a) Variations of RMSF along the amino acid
623 sequence for the apo, trunSUMO1- and preSUMO1-bound forms of SENP1. The two
624 exosite interface regions and three channel-lining loops are highlighted by shading in
625 mauve and orange, respectively. (b-c) Changes in RMSF upon binding trunSUMO1
626 and preSUMO1, displayed on the bound structures according to a color scale (shown;
627 red and blue corresponding to lower and higher flexibilities, respectively).

628

629 **Figure 4.** Comparison of experimental and calculated chemical shift perturbations

630 (CSPs) of SENP1 upon trunSUMO1 binding. (a) NMR results of Chen et al. (2014).
631 (b) Calculated results. Backbone amide CSPs are displayed according to a color scale
632 (red to gray corresponding to high to low CSPs); sidechain methyls with significant
633 CSPs (> 0.05 in panel a and > 0.08 in panel b) are shown as cyan sticks.

634

635 **Figure 5.** Results of community analysis for apo and trunSUMO1-bound SENP1
636 sim1, displayed on the left and right panels, respectively. Communities are displayed
637 either by different colors on the structures (upper row) or as numbered ovals with
638 matching colors (lower row). In the lower row, inter-community cumulative
639 betweennesses are displayed by the thickness of the lines connecting communities.
640 The community analysis was performed using the NetworkView plugin in VMD
641 (Sethi et al., 2009).

642

643 **Figure 6.** Reproduction of allosteric effects by restraining the exosite interface
644 regions of apo SENP1 at a widened separation. (a) Illustration of the restraint. Blue
645 arrows indicate the widening of the exosite cleft, and green dash indicates the
646 subsequent restraint. (b) Comparison of RMSFs between apo sim1 and the restrained
647 apo simulation. (c) Backbone amide and sidechain methyl CSPs of the restrained
648 simulation (to be compared with Figure 4b).

649

650 **Figure 7.** Illustration of the dock-and-coalesce mechanism for SENP-catalyzed
651 SUMO C-terminal cleavage. SENP is shown as two ovals (representing two
652 subdomains) connected by two strings, with the three channel-lining loops highlighted
653 as small circles; SUMO is shown as an oval (representing the β -grasp domain) with a
654 tail (the C-terminus). In the docking step, as the β -grasp domain wedges into the
655 exosite cleft, the cleft separation widens (indicated by red arrows), loopA and loopB
656 move (cyan and blue arrows) to make stronger inter-subdomain contact and also to
657 create space for docking the proximal portion of the SUMO C-terminus; the two
658 SENP subdomains lose flexibility on the fast timescale except for a distal region
659 (indicated by red to blue shading), and finally the proximal portion of the SUMO

660 C-terminus docks into the catalytic channel. Two hydrophobic pathways (bundles of
661 dashed arrows) propagate the allosteric effects from the exosite interface regions to
662 the catalytic center. In the coalescence step, the wedged β -grasp domain and the
663 docked C-terminus cooperate to reinforce allosteric effects, initiating inter-subdomain
664 correlated slow motions to allow for proper alignment of the substrate around the
665 catalytic center.

666

667 **Figure 2 – figure supplement 1.** Difference in conformational sampling among apo
668 SENP1 and two SUMO1-bound forms. (a) Conformational probability densities in the
669 plane of the first two principal components (PC1 and PC2), transformed into free
670 energy surfaces according to the Boltzmann relation. (b-c) Movements represented by
671 PC1 and PC2, respectively.

672

673 **Figure 2 – figure supplement 2.** Comparison of representative structures from
674 replicate simulations of different systems. An structure for apo SENP1 is overlaid to
675 those for the (a) trunSUMO1-bound and (b) preSUMO1-bound forms, by
676 superposition of the $\alpha 3$ and $\alpha 7$ helices. Apo SENP1 is shown in gray except with the
677 three channel-lining loops in orange and the two interface regions in mauve. These
678 portions are in red and green for the trunSUMO1-bound and preSUMO1-bound forms,
679 respectively.

680

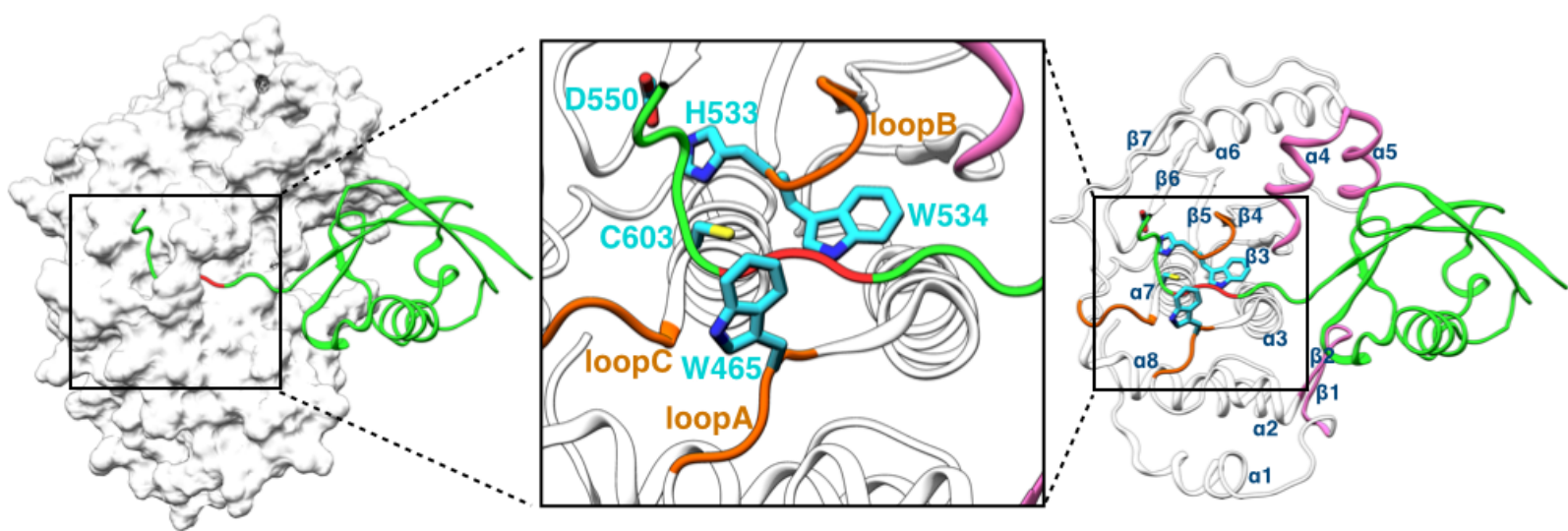
681 **Figure 5 – figure supplement 1.** Results of community analysis for apo and
682 trunSUMO1-bound SENP1 sim2. For caption, see Figure 5. Note that, for
683 trunSUMO1-bound SENP1, β -grasp residues in the lower interface (and upper
684 interface) are collected into community 3; hence the coupling between communities 1
685 and 6 seen in the other two replicate simulations is now part of the coupling between
686 communities 1 and 3.

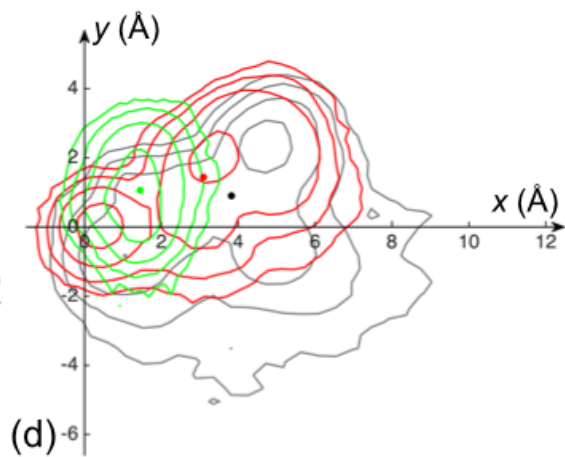
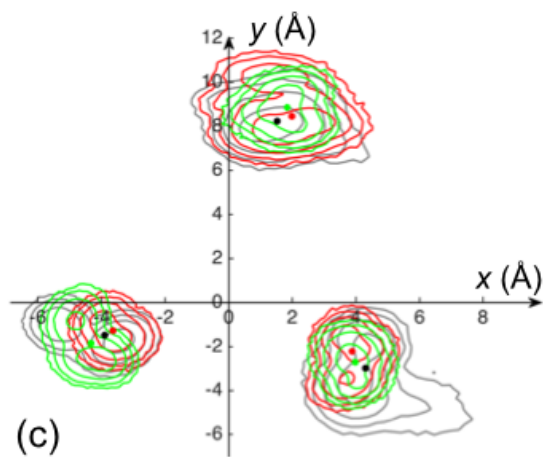
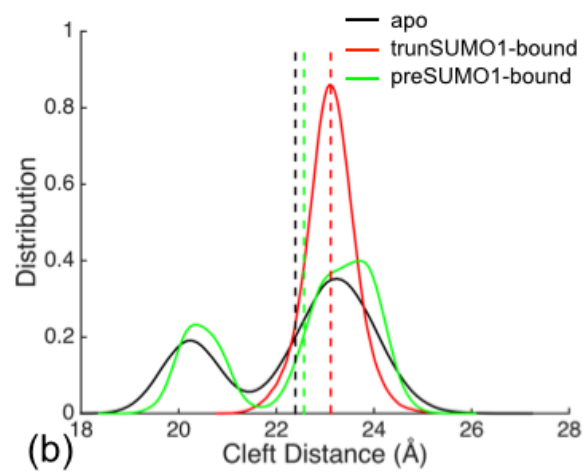
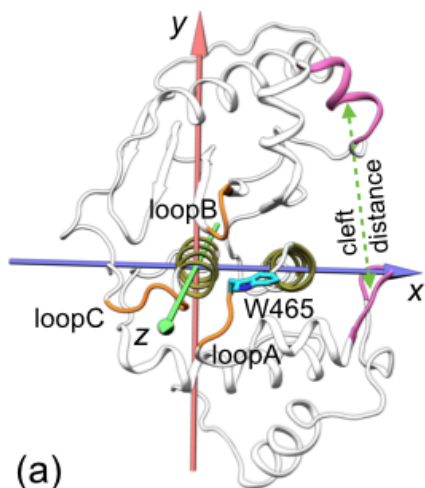
687

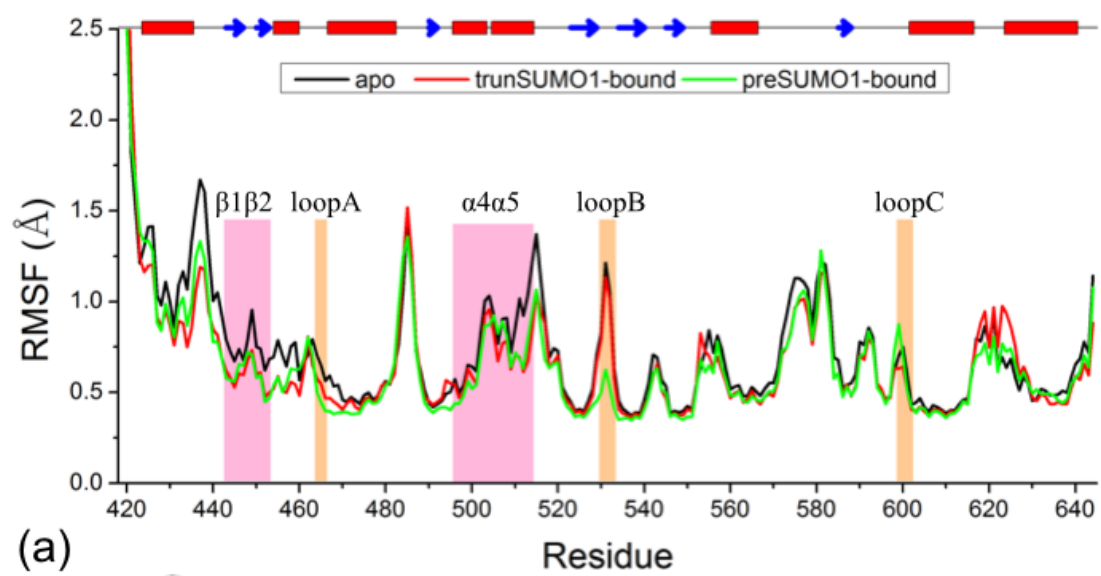
688 **Figure 5 – figure supplement 2.** Results of community analysis for apo and
689 trunSUMO1-bound SENP1 sim3. For caption, see Figure 5.

690

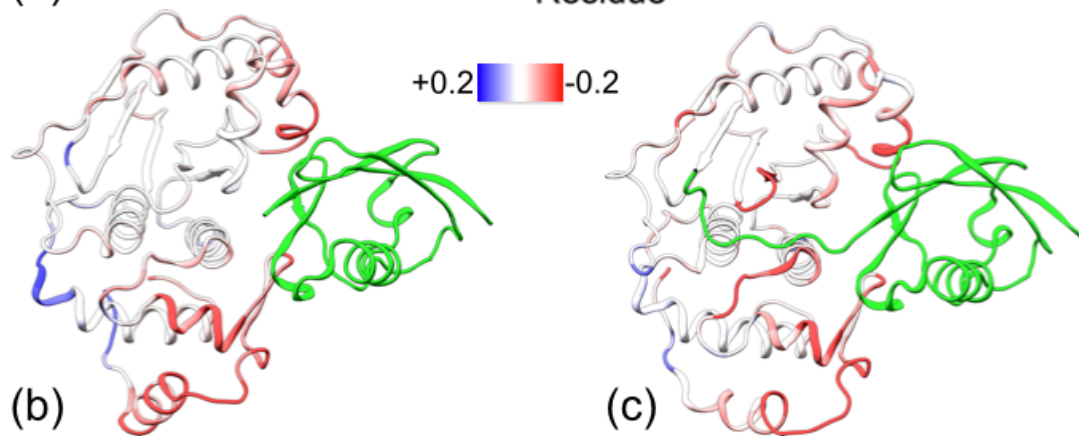
691 **Figure 6 – figure supplement 1.** The displacements of the channel-lining loops for a
692 control simulation in which the exosite interface regions of apo SENP1 are restrained
693 at a widened separation. (a) Distributions of the C α centers of the three loops in the
694 x - y plane. Results for apo sim1 and the restrained simulation are shown in black and
695 blue, respectively. The average positions of the loops in each system are shown as
696 dots. (b) Comparison of representative structures from apo sim1 and the restrained
697 simulation. For caption, see Figure 2 – figure supplement 2.







(a)



(b)

(c)

